



Interaction of electromagnetic fields with the environment/Interaction du champ électromagnétique avec l'environnement

Sea surface probing with L-band Doppler radar: experiment and theory

Marc Saillard^{a,*}, Philippe Forget^a, Gabriel Soriano^b, Maminirina Joelson^c,
Pierre Broche^a, Philip Currier^d

^a Laboratoire de sondages électromagnétiques de l'environnement terrestre, UMR CNRS, université du sud Toulon-Var, BP132, 83957 La Garde cedex, France

^b Institut Fresnel, UMR CNRS, université Paul-Cezanne, faculté St Jérôme, case 162, 13397 Marseille cedex 20, France

^c Climat sol environnement, UMR INRA, université d'Avignon, 33, rue Pasteur, 84000 Avignon, France

^d Degréane horizon, 730, rue de l'initiative, quartier St. Lazare, 83390 Cuers, France

Available online 30 August 2005

Abstract

In a first part, this paper describes radar experiments aimed at probing the sea surface from the coast. To capture small-scale changes in a coastal environment, a flexible high resolution, Doppler L-band radar with high resolution in range has been used. The data exhibit significant sensitivity to current and wind, which justifies the development of a model for inversion. The second part of the paper is thus devoted to our first attempt to model radar echoes, in order to accurately describe the influence of the geophysical parameters of interest. Here, the focus is put on waves generated by a local wind. The key point consists in taking properly into account non-linear hydrodynamic interactions between waves to generate a realistic moving sea surface. From the electromagnetic point of view, since standard low-frequency approximations no longer hold at L-band, a small-slope approximation has been implemented to compute the backscattered field. Numerical results show that for light winds (less than 5 m s^{-1}) the model correctly predicts the behaviour of the data with respect to wind speed and direction. **To cite this article:** *M. Saillard et al., C. R. Physique 6 (2005).*

© 2005 Académie des sciences. Published by Elsevier SAS. All rights reserved.

Résumé

Sondage de la mer par radar Doppler en bande L : expériences et théorie. Dans une première partie, cet article décrit une expérience destinée à sonder la surface de la mer à l'aide d'un radar côtier. Afin de saisir les fluctuations à petite échelle dues à l'environnement côtier, ce radar dispose d'une haute résolution en distance et fonctionne en mode Doppler en bande L. Les données ainsi enregistrées ont montré une sensibilité intéressante vis à vis du courant de surface ou du vent, justifiant le développement d'un modèle pour l'inversion. La seconde partie du papier est donc consacrée à notre première tentative pour modéliser l'écho radar, avec l'objectif de décrire correctement l'influence du vent local et des vagues qui y sont associées. Le point clé consiste à prendre en compte avec précision les interactions non-linéaires hydrodynamiques entre vagues pour engendrer des échantillons réalistes de surface de mer en mouvement. Sur le plan électromagnétique, comme les approximations basses-fréquences classiquement utilisées ne sont plus valables en bande L, nous avons mis au point une approximation faibles-pentes pour estimer le champ rétrodiffusé. Les résultats numériques montrent que pour des vents faibles (inférieurs à 5 m s^{-1}),

* Corresponding author.

E-mail address: marc.saillard@lseet.univ-tln.fr (M. Saillard).

le modèle décrit correctement le comportement des données en fonction de la force et de la direction du vent. *Pour citer cet article : M. Saillard et al., C. R. Physique 6 (2005).*

© 2005 Académie des sciences. Published by Elsevier SAS. All rights reserved.

Keywords: Remote sensing; Sea surface; Doppler spectra; L-band

Mots-clés : Télédétection ; Surface de mer ; Spectres Doppler ; Bande L

1. Introduction

This study has been motivated by the development of a coherent microwave radar to measure the properties of short surface waves, in the centimeter-decimeter range, which are very difficult to investigate by in-situ sensors. Recovery of surface characteristics from radar echoes also requires a forward model describing accurately the behaviour of the backscattered electromagnetic field with respect to geophysical parameters related to wind, current, fetch, swell, . . . In this paper, both experimental and numerical results are presented. Experimental data come from a L-band coherent radar (1.2 GHz), recording the backscattered electric field during a few seconds, which allows one to take benefit from the fluid motion, since waves moving at different speeds provide different Doppler frequency shifts. The square modulus of the Fourier transform of the radar echo is called Doppler spectrum and represents the basic information we refer to in this study.

Most of experimental studies only consider dual co-polarization modes VV and HH (vertical and horizontal transmission/reception, respectively), and not the cross-polarized components (VH and HV). It is well-known that HH and VV Doppler spectra may exhibit strongly different shapes, in particular as the incidence angle approaches grazing conditions [1–3]. The difference between HH and VV has been interpreted as the manifestation of bound waves and/or non-Bragg scattering effects due to, e.g., breaking waves. This study presents and interprets an original set of full-polarized data. Our motivation for recording also the cross-polarized components comes from our wish of vanishing the single scattering contribution, which strongly dominates the co-polarized signature at low winds, to clearly exhibit higher-order contributions. Data have been recorded under a great variety of meteorological conditions and have shown a sensitivity to environmental parameters that justifies the development of a model.

Much theoretical studies have been devoted to the behaviour of HH and VV radar cross-sections. They either address the three-dimensional problem through asymptotic scattering theories [4,5,2] or deal with a more rigorous formalism as applied to a simplified two-dimensional representation assuming the surface profile is invariant along one direction [6–8]. All these models tend to support the double contribution from non-linear interactions between water waves on one hand, purely electromagnetic effects on the other hand, to explain in particular the differences in Doppler shifts in HH and VV polarization modes. However, none of them can predict quantitatively the radar return, since asymptotic theories fail in the microwave frequency range and 2D models enforce wind and radar beam directions of propagation to coincide.

In this paper, 3D numerical simulations of radar Doppler spectra from sea surface at L-band are presented. To our knowledge, as far as Doppler spectrum is concerned, the present work constitutes the first attempt of 3D electromagnetic simulation. Following Toporkov et al. [7], a boundary integral electromagnetic method is combined with a Creamer non-linear surface [9].

The ocean surface simulation is carried out using a spectral method based on a semi-empirical sea surface spectrum. However, the influence of the non-linear hydrodynamic effects increases with radar frequency and led us to ‘undress’ this spectrum such that superimposing non-linear terms makes it match the original one. This was not necessary with HF and VHF radars, since roughness spectrum of longer waves is hardly modified. More details about this original part of the work are given in Section 3.

In the last part of the paper, simulations on directional Pierson-Moskowitz surface spectrum for 3 m s^{-1} wind speed are compared to data obtained under the same conditions.

2. The experiment

2.1. Description

The experiment was conducted near Toulon, south of France (Fig. 1). We used a coherent pulsed L-band radar designed and manufactured by Degréane Horizon. The radar can work with several transmitting/receiving antennas. Each antenna consists of an array of 8×8 25 dBi dipoles forming 8 parallel tubes disposed over a metallic panel. The main lobe of the radiation pattern is about 10° in width (3 dB). The radar system was operated on a concrete platform on a sheer cliff at an altitude of 91 m. Two pairs of vertically and horizontally polarized antennas were used. In the first experiment (Ex03), the antenna pairs

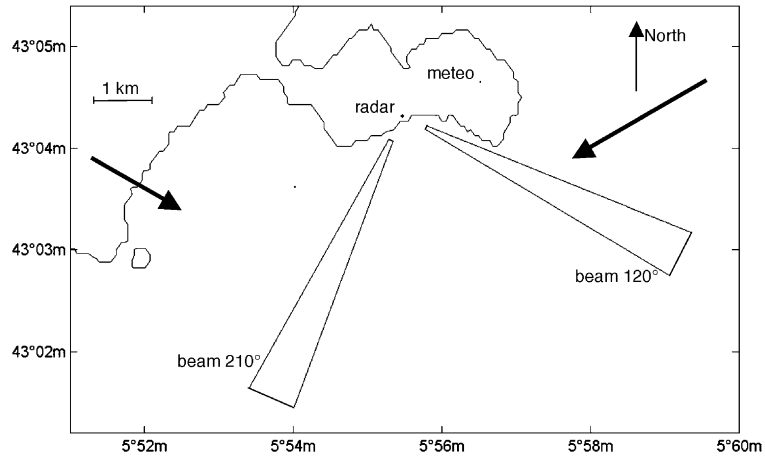


Fig. 1. Configuration of the experiment.

were pointing towards 120° from the geographic North and towards 210° , respectively. Each antenna was used in a monostatic way and provided co-polarized (HH or VV) radar echoes from the 2 orthogonal azimuths. In the second experiment (Ex04), all the antennas were pointing towards 120° . One pair was used for transmitting and the other one for receiving. Such a bistatic configuration allowed us acquisition of quad-polarized (HH, VV, VH and HV) radar echoes. Grazing incidence angle varied from about 12° to 1° with increasing distance.

Three main wind regimes were encountered: East-North-East winds (ENE) with high speeds (defined as $>5 \text{ m s}^{-1}$) up to 15 m s^{-1} , West-North-West (WNW) mistral winds with high speeds up to 21 m s^{-1} , and calm episodes ($<5 \text{ m s}^{-1}$) with varying wind direction. The wind directions for the first two regimes are drawn in Fig. 1. Wave measurements were also available. Ex03 is exhaustively described and main results are given in [10]. The results presented here include a preliminary analysis of Ex04 data.

2.2. Radar measurements

The characteristics of signal acquisition and processing were different in Ex03 and Ex04. Here, we just give an overview of these characteristics. A radar cycle consisted in four consecutive acquisitions: HH(120°), VV(120°), VV(210°) and HH(210°) for Ex 03; and VV (120°), VH(120°), HH(120°) and HV(120°) for Ex04. Incoherent summations of radar spectra were necessary to increase the number of degrees of freedom of spectral amplitudes, N , but in such a way that the total resulting radar cycle does not exceed the typical sea state and wind stationarity time scale, which is about 20 min. The effective radar cycles achieved by data processing were of this order of magnitude (20–35 min). For fixed inter-pulse period, IPP, important parameters of data processing are the number of sampled data points, n , and the number of coherent integrations, NCI. n and NCI values govern the Doppler frequency bandwidth, Δf_D , and resolution, δf_D . During Ex03, NCI and n were not always optimized regarding the exact bandwidth and resolution needed. This problem was overcome during Ex04 by significantly increasing n (up to 2048 instead of 128 for Ex03), at the expense, for reasons of memory, of the number of radar cells. For Ex04, incoherent summations of consecutive spectral amplitudes were done in order to have a constant Doppler velocity resolution and, here too, to increase N .

2.3. Morphology of Doppler spectra

At low winds, the dominant features of the HH and VV spectra (top of Fig. 2) are similar to what could be observed in HF [11,12], VHF [13] and X-band [14], with the same coarse resolution. The energy is concentrated in the vicinity of Bragg frequencies, $\pm f_B$, with f_B given by $2\pi f_B = (2gk)^{1/2}$, g the gravity acceleration and k the electromagnetic wavenumber. The asymmetry of the spectra is mainly governed by the direction of the wind that generates the wave field. Compared to HH and VV modes, spectra associated with cross-polarized components are flattened in the vicinity of Bragg frequencies, since the main contribution to the so-called Bragg lines comes from single scattering, in the sense that a single spatial frequency of the surface profile is responsible for it. Let us recall that such a process does not contribute to the cross-polarized radar cross-section. It is also interesting to notice that the latter is of same order of magnitude as the HH cross-section, but much smaller than the VV one under grazing incidence.

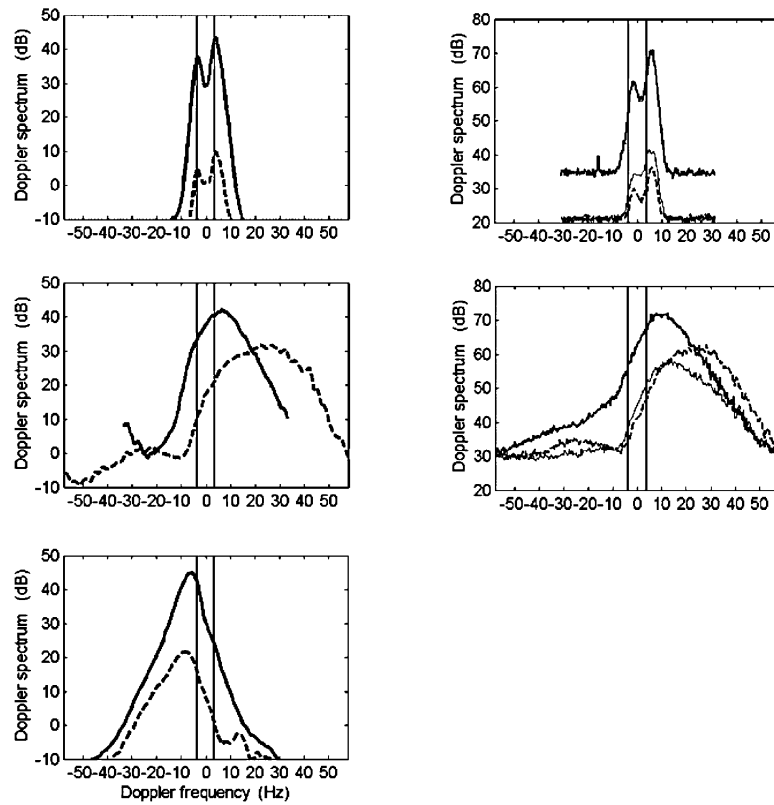


Fig. 2. Doppler spectra for various wind directions and strengths. Solid lines: VV polarization. Dashed lines: HH. Grey lines: VH. Top left: low wind, Ex03. Top right: low wind, Ex04. Middle left: strong ENE wind, Ex03. Middle right: strong ENE wind, Ex04. Bottom left: strong WNW wind, Ex03.

For strong ENE and WNW winds (middle and bottom of Fig. 2, respectively) spectra are much wider than for low winds with a bandwidth depending on the wind direction. A characteristic of Doppler spectra in VV is the consistency of the asymmetry of these spectra with the wind direction as was observed in low wind situations. These results suggest that, as in the low wind case, Doppler spectra in VV are mainly governed by radar waves – ocean waves interaction processes of Bragg type. Doppler spectra in HH can differ significantly from spectra in VV. The main differences concern the shape which is often characterized by a wide bell-shaped peak and the position of the maximum showing higher Doppler frequencies than in VV. These differences depend on the radar look direction. Following the terminology of [1] Doppler spectral peaks can be ‘fast’ or ‘slow’ depending on the shift of the maximum from Bragg frequencies implying a departure of radar waves-ocean waves interaction processes from the Bragg regime. Under ENE wind conditions, when the asymmetry of the spectrum in VV is important due to quasi-up-wind conditions, the fast scatterers responsible for the corresponding HH spectrum also contribute to enrich the VV radar return at high Doppler frequencies, but with a less important relative contribution. HV and VH spectra are almost identical both in shape and magnitude. Again, differences with co-polarized spectra can be observed in the vicinity of Bragg frequencies. Furthermore, from a preliminary investigation, it seems that the influence of fast scatterers is qualitatively similar to what was observed for VV spectra.

3. Ocean surface model

Modelling L-band radar Doppler spectra from the ocean requires an accurate description of sea surface motion. This is a difficult, challenging task because the sea surface is very complex due to, in particular, non-linear wave interactions and randomness aspects.

Linearizing hydrodynamic equations would lead to represent the sea surface as a superposition of independent harmonic waves, referred to as a ‘linear’ sea surface. In this case, describing motion of sea surface is straightforward from the knowledge of the dispersion relation of free gravity waves (contribution of capillary waves at L-band is negligible) and of the associated part

of the sea surface spectrum. But it is well known that interactions between harmonic waves play an important role in Doppler spectra signature of sea surface. The usual method used to solve this problem consists in applying a perturbative approach. A linear surface is first generated and higher order corrections are obtained from expansion of hydrodynamic equations. Such terms fill the lack of phase relationships between waves, which is known to be the signature of the non-linear character. However, keeping in mind that wave models are semi-empirical, thus take all wave interactions into account, this approach implicitly assumes that higher order terms do not significantly modify the part of the surface spectrum that contributes to the radar echo. This is verified up to the VHF radar frequency range for which the method has yielded to satisfactory results, but not at higher frequencies.

In L-band remote sensing, it appears that if all the energy is put into the linear surface, the second order term would create a significant energy bias in the sub-metric wavelength range. Therefore, the spectrum describing the linear part of the surface has to be built such that adding higher order terms leads to the chosen semi-empirical surface spectrum.

3.1. Linear simulation

Let us denote by $P(\mathbf{k})$ the two-dimensional wave spectrum, where \mathbf{k} is the spatial wavenumber of polar coordinates (k, θ) . As a first approach, a directional Pierson–Moskowitz (hereinafter noted as PM) spectrum function

$$P(\mathbf{k}) = \psi_{PM}(k) \cdot \phi(\theta) = \frac{\alpha}{k^4} \exp\left(-\frac{5}{4} \left(\frac{k}{k_p}\right)^2\right) \mathcal{N} \left| \cos^5\left(\frac{\theta - \theta_v}{2}\right) \right| \tag{1}$$

is considered. The PM spectrum depends on two parameters $\alpha = 4.05 \times 10^{-3}$ and the spectrum peak wavenumber k_p which is function of the wind speed. In Eq. (1), θ_v represents the wind orientation angle, and \mathcal{N} is a normalization factor.

The discretized form of the linear surface can be written as:

$$\eta_t(\mathbf{x}) = \text{Re} \sum_{\mathbf{k}} A_t(\mathbf{k}) e^{i\mathbf{k} \cdot \mathbf{x}} \tag{2}$$

with $A_t(\mathbf{k}) = \gamma(\mathbf{k}) \sqrt{2P(\mathbf{k})} \delta k_x \delta k_y e^{-i\omega t}$, where ω is deduced from the dispersion relation of gravity waves $\omega^2 = g|\mathbf{k}|$ and γ is a complex Gaussian process. The computation can be efficiently performed thanks to an inverse Fast Fourier Transform (FFT).

3.2. Non-linear simulation

An approach to carry out non-linear hydrodynamic models involves perturbation techniques around the water surface level at rest to determine higher order corrections to the linearized solution. This was used successfully in the past by different authors, e.g., in [15]. However, implementation of these models is of high numerical cost (N^2), preventing their use for a Monte Carlo simulation.

Another possibility to insert non-linear effects is the Hamiltonian formalism under the weak wave-turbulence theory, of which extensive application has been made in the fields of water surface waves since the fundamental work of [16]. In this study, we will consider a recent formulation of the Hamiltonian formalism as given by [9], also recently used by Toporkov et al. in a two-dimensional model.

The Cremer formulation writes as a non-linear transformation of the Hilbert transform of the linear surface. At a given time t , the Hilbert transform, derived from (2), can be expressed

$$\mathbf{h}_t(\mathbf{x}) = \text{Re} \sum_{\mathbf{k}} \left(-i \frac{\mathbf{k}}{k}\right) A_t(\mathbf{k}) e^{i\mathbf{k} \cdot \mathbf{x}} \tag{3}$$

thus can be computed by FFT, at a $N \log N$ cost. The Cremer non-linear transform is defined as

$$C_t(\mathbf{k}) = \frac{1}{N} \sum_{\mathbf{k}} \frac{\exp(i\mathbf{k} \cdot \mathbf{h}_t(\mathbf{x})) - 1}{k} e^{-i\mathbf{k} \cdot \mathbf{x}} \tag{4}$$

However, this transform cannot be computed by FFT, since the term $\exp(i\mathbf{k} \cdot \mathbf{h}_t(\mathbf{x}))$ depends on both \mathbf{k} and \mathbf{x} , and reveals to have also a N^2 numerical cost. To circumvent these difficulties, the exponential is expanded as a series. Then, the non-linear transform writes $C_t = \sum_{n \geq 1} C_t^n$, where C_t^1 identifies with A_t , that is, with the linear surface, while the second order term is given by three FFT

$$C_t^2 = -\frac{k_x^2}{2k} \mathcal{F}^D[h_{t_x}^2] - \frac{k_x k_y}{k} \mathcal{F}^D[h_{t_x} h_{t_y}] - \frac{k_y^2}{2k} \mathcal{F}^D[h_{t_y}^2] \tag{5}$$

Table 1
 Statistics of a generated surface of area $100\lambda \times 100\lambda$ and $N = 512 \times 512$ sampling points for a 3 m s^{-1} wind speed ($k_p = 0.73 \text{ rad s}^{-1}$) and a wind direction $\theta_v = 0^\circ$

Surface	Root mean square		
	Height	Slope (x)	Slope (y)
Linear	55.25 mm	0.102	0.081
Creamer(2)	55.50 mm	0.146	0.112

Therefore, a second order Creamer surface can be obtained by performing FFT only, through $\eta_t = \text{Re } \mathcal{F}^I[A_t + C_t^2]$. In order to emphasize the non-linear effects, the statistical parameters of both the linear and non-linear simulations are reported in Table 1.

As applied to a linear surface profile derived from the PM spectrum, it appears that the rms height remains unchanged but that the rms slope is strongly increased, by about 50 percent, which translates an unrealistic magnification of the small scale roughness.

3.3. ‘Undressing’ spectrum function

In order to correct this artifact about the small scale behaviour, a fictitious ‘linear’ sea surface spectrum should be used as an input of the model, instead of the semi-empirical spectrum. In our opinion, there is no clear method in hydrodynamic theory that allows someone to cast the semi-empirical sea spectra available in the literature into linear and non-linear contributions. The present procedure is thus empirical. To avoid energy bias in our models, we propose an ‘undressed’ spectrum ψ_u , where the small scale component energy level has been reduced, such that the resulting surfaces possess the same height and slopes root mean squares as the linear PM surface.

$$\psi_u(k) = \begin{cases} \psi_{\text{PM}}(k), & k < k_c \\ \beta k^{-p}, & k > k_c \end{cases} \quad (6)$$

For wavenumbers higher than k_c , this spectrum decreases faster than the PM spectrum. Coefficients k_c and p are determined numerically and $\beta = k_c^p \psi_{\text{PM}}(k_c)$ ensures the continuity of the spectrum at $k = k_c$.

4. Electromagnetic scattering model

The experimental Doppler spectra are wider than those predicted by the classical second-order model established by Barrick [5]. The discrepancy results from the large rms height of sea surface, which exceeds the limit of validity of the electromagnetic perturbation theory, roughly estimated to a twentieth of the incident wavelength. Obviously, more general formulations are required. As a good candidate is another class of statistical methods, dedicated to the scattering from rough surfaces with small slopes, like the ocean surface [6]. However, at lowest order, such methods do not provide an estimation of cross-polarization, and computing higher order terms requires integration of rapidly oscillating functions, hard to perform accurately. Rino et al. [17], Toporkov and Brown [18] have shown how a rigorous integral equation-based numerical method can be applied to time-varying surfaces. However, deriving a Doppler spectrum associated with one surface sample requires the computation of some hundreds of time-harmonic scattered fields, one for each time step, and a statistical result is typically obtained by averaging over a hundred Doppler spectra, making the simulation numerically intensive. Such an approach to address the three-dimensional problem requires a *fast* solver. In the framework of a boundary integral formalism associated with a moment method and a Monte Carlo process, our approach combines a small slope approximation with a fast numerical method, as described in [19]. It is based on the Meecham–Lysanov approximation [20], which consists in approximating the true distance between two surface points by their horizontal distance. Therefore, if a regular mesh grid is used, the matrix reveals a two-dimensional Toeplitz structure, allowing the use of FFT to perform matrix-vector products through the iterative solver. The computing time and RAM required by the method scale as $N \log N$ and N , respectively.

In addition, for reflecting materials, like ocean water at microwave frequencies, the lower medium Green’s function shows a fast exponential decreasing behaviour, leading to a short range integral relationship between electric and magnetic currents. Approximating this operator by a local impedance [21], which depends on the skin depth and on the local curvatures, reduces the number of unknowns by a factor of 2.

The incident field is a Gaussian beam, to ensure fast decay of the incident field away from the central part of the illuminated zone and avoid edge effects resulting from the limited sampled area. However, at grazing incidence, the minimum enlightened two-dimensional surface, thus the number of unknowns scales as θ_g^{-3} , $\theta_g = \pi/2 - \theta_i$ being the grazing angle. This drastically

limits the range of incidence angles that can be investigated. Overcoming this limitation would require the use of different integral equations and incident field.

5. Numerical results

At the electromagnetic frequency of 1.2 GHz ($\lambda = 0.25$ m), the relative permittivity of sea water is approximately $\varepsilon = 73.5 + i61.0$ for standard values of temperature and salinity. Surface samples dimensions should be larger than the wavelength of the longest water wave $\lambda_p = 2\pi/k_p$, that is around 15 m for a 4 m s^{-1} wind speed. Samples are square surfaces of 25 m sides (100λ), sampled with 512 points in each direction. Incidence is set to the maximum value for such a surface length, that is 70° . The backscattered field is recorded during $N_t = 128$ time steps of $\delta t = 40$ ms, and the Monte Carlo average is performed with 48 samples.

Fig. 3 compares the Doppler spectra for a linear PM surface with 3 m s^{-1} wind speed and for its associated Creamer(2) non-linear surface derived from the undressed spectrum (6). Only co-polarized components are plotted. One can notice that hydrodynamic non-linearities make the Doppler spectra smoother and that the main lobes around Bragg frequencies $f_B \simeq \pm 3.4$ Hz are broadened. The increase of the backscattered energy results from the changes in height and slope distributions. Even though the rms remain unchanged, larger slopes are observed at the top of the waves. Two peaks surrounding each Bragg peak remain observable in VV polarization, occurring at $f = \pm f_B \pm f_p$, with $f_p = \sqrt{gk_p}/(2\pi) \simeq 0.4$ Hz, as predicted by the second order terms of perturbation theory. Finally, for comparison, we have found a rather long period with stable wind speed and direction, almost constant surface current and with no swell superimposed to wind waves. Indeed, interaction of such long waves with wind waves also contributes to broadening the main lobes of the spectra, and, up to now, this has not been included in models. Averaging the recorded spectra of 14 December 2004, from 12 to 15 h, with measured ENE wind speed oscillating between 2 and 3 m s^{-1} , wind direction between 40 and 70° from radar look direction 120 , makes the comparison with computed spectra, for wind speed 3 m s^{-1} and 60° angle, significant. Fig. 4 shows VV, VH and HH spectra from top to bottom. It must be emphasized that real and synthetic data have been vertically shifted, but not in the same way. Indeed, let us recall that the incidence angle is not the same, 70° in our computations and about 86.5° at 1.4 km range for the data. Therefore, neither the backscattered cross-sections nor the polarization ratios can coincide. Vertical shifts have also been adjusted to separate the curves, especially HH and VH, which are of same order of magnitude. Nevertheless, this comparison shows that the shape of the spectra predicted by the model fits quite well the data. The behaviour of the model with respect to geophysical parameters such as wind direction and speed has been investigated for wind speeds up to 4 m s^{-1} and it has been checked that it coincides with that of the data.

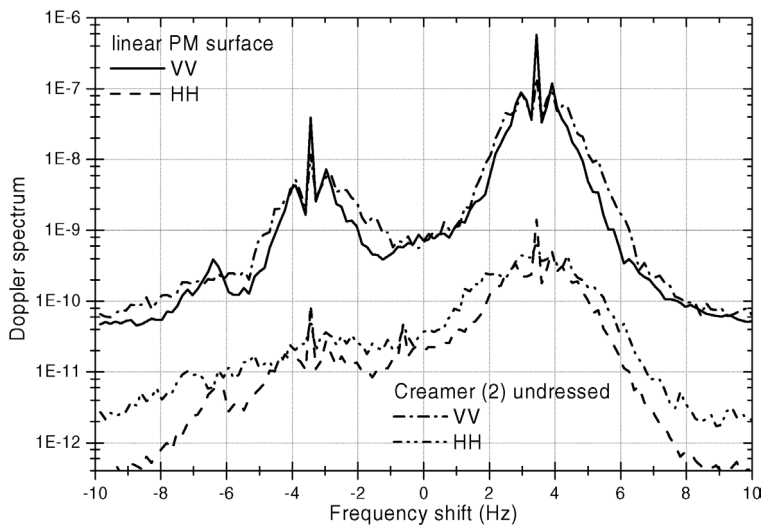


Fig. 3. Comparison between the linear PM and the Creamer (2) undressed surface co-polarized Doppler spectra.

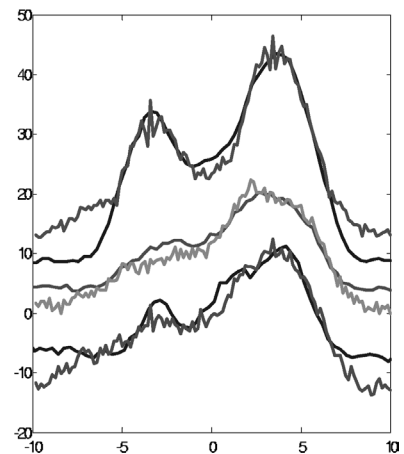


Fig. 4. Comparison between data and the modeled Doppler spectra versus frequency shift (Hz). To avoid overlapping, the curves have been vertically shifted. Smooth curves: data; oscillating curves: computations. Top: VV; middle: VH; bottom: HH.

6. Conclusion

L-band Doppler spectra for light winds exhibit a morphology that is consistent with interaction processes of Bragg type between electromagnetic waves and surface gravity waves. The shift of the maximum from Bragg wave velocity can be explained by surface current effects. The non-Bragg scattering mechanisms occurring for strong winds are dominant in HH mode while their contribution is much smaller than that of Bragg mechanism in VV polarization, the cross-polarization VH/HV exhibiting an intermediate behaviour.

Combining a perturbative approach to describe hydrodynamic non-linearities with a semi-empirical surface spectrum associated with wind waves, moving sea surface samples have been generated for light winds. It appears that, in the micro-wave frequency range, it is necessary to damp the energy of high frequencies in the empirical spectra before introducing non-linear effects. Otherwise, their contribution is strongly overestimated.

Computation of the radar echo is achieved at reasonable computational cost thanks to a small slope approximation of the kernel of a boundary integral equation, which permits us to estimate both co- and cross-polarization contributions. This 3D model and the data behave in the same way with respect to wind speed and direction, and Doppler spectra present very similar shapes at low wind, whatever the polarization.

References

- [1] P.H.Y. Lee, *J. Geophys. Res. C* 100 (1995) 2591–2611.
- [2] W. Plant, *J. Geophys. Res. C* 102 (1997) 21131–21146.
- [3] W. Plant, W.C. Keller, V. Hesany, T. Kara, E. Bock, *J. Geophys. Res. C* 104 (1999) 3243–3263.
- [4] F.G. Bass, I.M. Fuks, *Wave Scattering from Statistically Rough Surfaces*, Pergamon, New York, 1979.
- [5] D.E. Barrick, B.L. Weber, *J. Phys. Oceanogr.* 7 (1977) 11–21.
- [6] J.T. Johnson, J.V. Toporkov, G.S. Brown, *IEEE Trans. Geosci. Remote Sensing* 39 (2001) 2411–2420.
- [7] J.V. Toporkov, G.S. Brown, *IEEE Trans. Antennas Propagat.* 50 (2002) 417–425.
- [8] A.R. Hayslip, J.T. Johnson, G.R. Baker, *IEEE Trans. Geosci. Remote Sensing* 41 (2003) 2287–2293.
- [9] D.B. Creamer, F. Henyey, R. Schult, J. Wright, *J. Fluid Mech.* 205 (1989) 135–161.
- [10] P. Forget, M. Saillard, P. Broche, *J. Geophys. Res.* (2005), in press.
- [11] D.E. Barrick, *Remote sensing of sea state by radar*, U.S. Gov. Printing Office, Washington, DC, 1972.
- [12] P. Forget, et al., *Radio Sci.* 16 (1981) 917–925.
- [13] P. Broche, P. Forget, J.C. de Maistre, J.L. Devenon, M. Crochet, *Radio Sci.* 22 (1987) 69–75.
- [14] G.R. Valenzuela, *J. Geophys. Res. C* 79 (1974) 5031–5037.
- [15] G.R. Valenzuela, *Boundary Layer Meteorolog.* 13 (1978) 61–85.
- [16] V.E. Zakharov, *J. Appl. Mech. Tech. Phys.* 51 (1968) 269–306.
- [17] C.L. Rino, T.L. Crystal, A.K. Koide, H.D. Ngo, H. Guthard, *Radio Sci.* 26 (1991) 51–71.
- [18] J.V. Toporkov, G.S. Brown, *IEEE Trans. Geophys. Remote Sensing* 38 (2000) 1616–1624.
- [19] M. Saillard, G. Soriano, *IEEE Trans. Antennas Propag.* 52 (2004) 2799–2802.
- [20] A.G. Voronovich, *Wave Scattering from Rough Surfaces*, Springer-Verlag, Berlin, 1994.
- [21] A.M. Marvin, V. Celli, *Phys. Rev. B* 50 (1994) 14546–14553.